MoS_2/Epitaxial graphene layered electrodes for solid-state supercapacitors

Mojtaba Amjadipour [1], *Jonathan Bradford* [2,3], *Negar Zebardastan* [2,4], *Nunzio Motta* [2,4], *and Francesca Iacopi* [1,5]*

[1] School of Electrical and Data Engineering, Faculty of Engineering and Information Technology, University of Technology Sydney, NSW, Australia.

[2] School of Chemistry and Physics, Science and Engineering Faculty, Queensland University of Technology, QLD, Australia.

[3] School of Physics & Astronomy, University of Nottingham, Nottingham, NG7 2RD, United Kingdom.

[4] Centre for Materials Science, Queensland University of Technology, QLD, Australia

[5] Centre for Clean Energy Technology, University of Technology Sydney, NSW, Australia.

* Corresponding author.
E-mail: francesca.iacopi@uts.edu.au

Keywords

quasi-solid-state supercapacitors, epitaxial graphene, MoS_2, 3C-SiC

Abstract

The potential of transition metal dichalcogenides such as MoS_2 for energy storage has been significantly limited so far by the lack of conductivity and structural stability. Employing highly conductive, graphitic materials in combination with transition metal dichalcogenides can address this gap. Here, we explore the use of a layered electrode structure for solid-state supercapacitors, made of MoS_2 and epitaxial graphene on cubic silicon carbide for on-silicon energy storage. We show that the energy storage of the solid-state supercapacitors can be significantly increased by creating layered MoS_2/graphene electrodes, yielding a substantial improvement as compared to

electrodes using either epitaxial graphene or MoS_2 alone. We conclude that the conductivity of epitaxial graphene and the growth morphology of MoS_2 on graphene play an enabling role in the successful use of transition metal dichalcogenides for on-chip energy storage.

1. Introduction

Electrochemical supercapacitors are key components of advanced energy storage systems. Their long life cycle, low maintenance requirements, and capability to deliver high power densities make supercapacitors complementary to conventional batteries [1-6]. Charge storage in electrochemical supercapacitors relies principally on the presence of an electrical double layer at the electrode/electrolyte interface [4, 7]. Redox reactions or pseudocapacitance can also contribute to charge storage [4, 7, 8].

Two-dimensional transition metal sulfide (TMS) materials have recently emerged, holding, among others, high promise for energy storage applications [9-14]. These advanced layered materials present outstanding double-layer performance thanks to their high surface area and the presence of interlaminar sites for charge storage [14-18]. However, their implementation in energy storage systems has been challenged by the lack of structural stability and low conductivity [19, 20]. One of the possible ways to overcome these limitations is the combination of TMS with a material like graphene [16, 19-23]. Graphenic materials could contribute to the missing structural stability and high electrical conductivity to the thin-layered electrodes [19, 20, 24]. The efficient and scalable fabrication of graphene and TMS hybrid structures could determine the future applications of TMS materials in energy storage.

To date, graphene oxide (GO) and graphene flakes have been explored in combination with TMS for composite structures for energy storage applications [19, 22, 24-29]. Da Silveira Firmiano et al. [19] proposed MoS_2/GO composite electrodes and demonstrated that the composite structure leads to a significant capacitance performance improvement. Ji et al. [22] fabricated a flexible supercapacitor based on MoS_2/GO composite electrodes using ball milling of bulk MoS_2 and GO powders. They demonstrated that the composite electrodes improve the capacitance by up to 50% (at 0.5 Ag^{-1}) compared to the bulk MoS_2 ones [22].

While GO and graphene flakes provide a promising platform for flexible energy storage device fabrication [1, 22], epitaxial graphene (EG) directly grown on silicon substrates offer substantial advantages for on-chip supercapacitors [7, 30-36]. The EG on silicon technology is underpinned by a metal-based catalytic wafer-scale growth of graphene using cubic silicon carbide on silicon, which can be compatible with the current semiconductor manufacturing [31, 35, 37-41]. This binder-free method is capable of producing EG with tunable characteristics and high adhesion to the substrate, which also has the potentials for miniaturization and wafer-level production [39, 40]. Pradeepkumar et al. [40] have recently demonstrated that the alloy-mediated graphitization approach maintains an epitaxial relation of graphene with the substrate; it also leads to a large area epitaxial graphene coverage. No data is available to date on the use of layered TMS/EG electrodes for miniaturized, integrated energy storage applications. In the present study, we explore the electrochemical performance of MoS_2/EG layered electrodes directly grown on a silicon substrate.

2. Experimental methods

2.1 Materials preparation

3C-SiC (cubic polytype) films epitaxially grown on Si (100) substrates have been acquired from NOVASiC. The films underwent a chemical - mechanical polishing procedure (StepSiC® by NOVASIC (France)) [42, 43]. The final SiC epi layer thickness is ~500 nm. A catalytic alloy method was employed to grow EG on the SiC films [37, 38]. A combination of a Ni layer (~10 nm) followed by a Cu layer (~ 20 nm) was used to fabricate epitaxial graphene. A Cryopump deposition chamber operating with CD Ar^+ ion and 200 mA current was employed for sputtering the metallic layers. Annealing the metal-coated samples at ~1100 °C for an hour under vacuum condition (~10^{-5} mbar) leads to breaking of the Si-C bonds and the release of the carbon atoms which can form epitaxial graphene on the surface. Ni silicides are the by-product of this procedure, which were later removed with any metal residues on the surface using chemical wet etching for about nine hours (Freckle solution) [37, 38].

MoS_2 was grown by chemical vapor deposition (CVD) directly on the EG/3C-SiC/Si(100) substrates. The substrates were placed in a horizontal quartz tube furnace, 3 cm downstream from an alumina boat with 30 mg of MoO_3 powder. Another crucible with 1.5 g of sulfur powder was placed 20 cm upstream in a separate heating zone. Prior to the growth, the tube was pumped to ~70 Torr under 600 sccm Ar and purged for 1 hour to remove residual air. At the beginning of the growth process, the Ar flow rate was reduced to 200 sccm. The MoO_3 was first heated at 150 °C for 20 minutes to remove any adsorbed water, before ramping to 800 °C to evaporate the MoO_3 precursor. The sulfur precursor was heated simultaneously to 280 °C with a similar ramp. Both zones were held at their respective temperatures for a growth time of 20 min before cooling naturally under Ar flow.

2.2 Device fabrication

A sandwich cell design using two electrodes (~2×1 cm^2) with a gel electrolyte in between the electrodes was used to fabricate the quasi-solid-state supercapacitors [44]. PVA+H_2SO_4 gel electrolyte was prepared by mixing 1 g PVA molecule (108K molecular weight) and 10 mL deionized water followed by the addition of 1g H_2SO_4 (98%). The mixture was vigorously stirred at 80 °C for a few hours to become completely transparent. Kapton tape was used to seal the cells obtaining a typical gel electrolyte thickness of ~300 µm.

2.3 Characterization

A Zeiss Supra 55VP scanning electron microscope (SEM) and Park XE7 atomic force microscope (AFM) were employed for imaging the surface. Raman spectra were collected by a WiTec Raman microscope using a 532 nm green laser; the spectra presented in this paper are obtained by averaging 2500 single spectra collected over a 100 μm^2 area map. X-ray photoemission spectroscopy (XPS) measurements were acquired using a Kratos Axis Supra instrument with a monochromated Al K_α X-ray source ($h\nu = 1486.7$ eV).

An electrochemical workstation (CH Instruments, 660 E Model) was used to assess the electrochemical performance of the cells operating in a two-probe configuration. Galvanostatic charge/discharge (CD) measurements were conducted with 1 V potential window and 1-5 µA current. The stability of the cells over long cycles was assessed using the CD test over 10000 cycles by 10 µA current and 1 V potential window. The electrode areal specific capacitance (C) was calculated based on the CD test results using the equation

$$C = 4I\Delta t / \Delta U, \qquad (1)$$

where C is the areal specific capacitance in (μFcm^{-2}), I represents the current density (μAcm^{-2}), Δt is the discharge time (s), and ΔU is the potential window (V). Data reported here are the averaged values calculated from 5 to 10 charge/discharge cycles. Electrochemical Impedance Spectroscopy measurement conducted in the 0.01 Hz to 100 kHz frequency range with a signal amplitude of 5 mV.

3. Results and discussion

MoS_2 has been synthesized on two different surfaces: bare 3C-SiC/Si and EG grown on 3C-SiC/Si. **Figure** 1 shows the SEM images of the samples before and after the MoS_2 growth. Pristine SiC presents a flat surface with a roughness root mean square (RMS) value of ~5 nm (**Figure 1a & S3a**), while the EG growth using the catalytic alloy method increases the roughness RMS to ~25 nm (**Figure 1c & S3c**). The MoS_2 synthesis on both of these surfaces leads to the formation of the MoS_2 crystals evident in the SEM micrographs (**Figure 1b & d**). As a result, the surface roughness increases substantially in both cases after MoS_2 growth. The AFM measurements indicate ~44 nm RMS for the growth on bare 3C-SiC and ~54 nm RMS for the growth on EG; however, we anticipate that those values may not reflect the actual roughness of the final surfaces as the radius of curvature of the AFM tip (~30 nm) would substantially distort (**Figure S3b & d**) the morphology of the MoS_2 (**Figure S1a & b**). The SEM micrographs clearly indicate that the MoS_2 crystals grown on the EG surface are denser. Also, the MoS_2 tends to grow with a rather random crystal orientation on the bare SiC substrate (**Figure 1b and S1a**), while the MoS_2 crystals appear predominantly standing vertically on the EG surface (**Figure 1d and S1b**). The estimated thickness of grown MoS_2 crystals from **Figure S1b** is 30-50 nm.

Fei et al. [45] had illustrated the effect of the growth temperature on the orientation of the MoS_2 crystals, indicating that the low-temperature growth of MoS_2 results predominantly in a vertical alignment. The surface energy and template of the substrate used for the MoS_2 growth are expected to have a significant effect on the morphology of the MoS_2 layer as well [46-48]. Here we believe that the low surface energy of the EG layer leads to the vertical alignment of the MoS_2 crystals. In fact, when the growth of MoS_2 takes place on a defective EG surface, the MoS_2 layer does not have the same aligned vertical orientations as seen in the high-quality EG surface, and its coverage is poor (**Figure S2**).

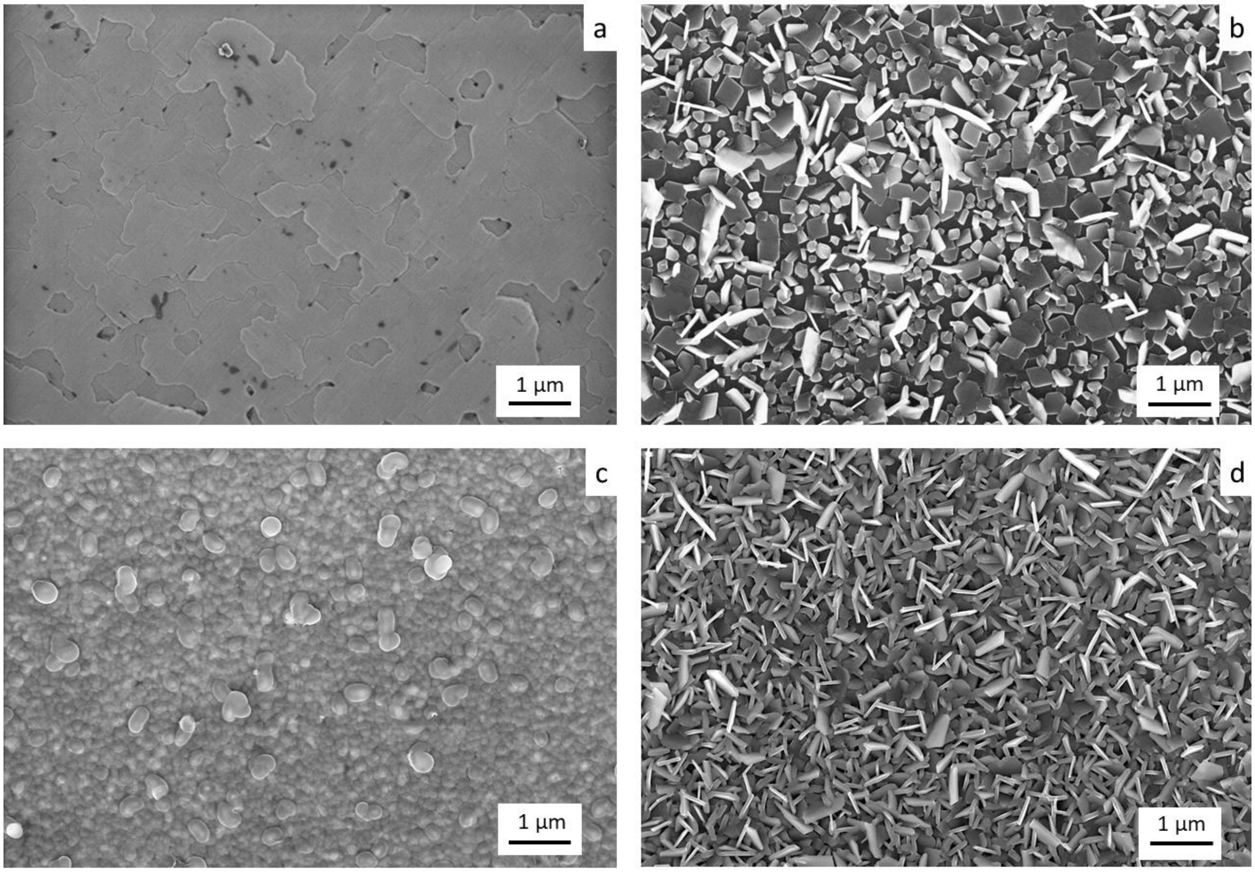

Figure 1. SEM images of (a) pristine 3C-SiC/Si substrate, (b) MoS_2 synthesized on the 3C-SiC/Si, (c) EG grown on 3C-SiC/Si substrate, (d) MoS_2 grown on the EG electrodes.

Figure 2a shows the Raman spectra of the pristine 3C-SiC/Si substrate; two main notable peaks are the Si peak at ~520 cm^{-1} and the LO peak of SiC at ~970 cm^{-1} [49, 50]. After MoS_2 synthesis on the SiC surface, two dominant peaks E_{2g} at ~378 cm^{-1} and A_{1g} at ~404 cm^{-1} appear (**Figure 2b**), which correspond to in-plane and out-of-plane vibrational modes of hexagonal MoS_2 crystal, respectively [51, 52]. The Raman spectra of the EG sample have three extra peaks, which originate from graphene lattice: D peak at ~1340 cm^{-1}, G peak at ~1580 cm^{-1}, and 2D peak at ~2680 cm^{-1}

(**Figure 2c**) [53, 54]. The D peak arises from defects within graphene lattice. The intensity ratio between D and G peaks has been widely used as a measure to compare defect density for graphene-based materials [53, 54]. The intensity ratio of I_{LO}/I_{2D} also indicates the graphene coverage over the 3C-SiC/Si substrate; lower values correspond to higher coverage. Here I_D/I_G is ~0.2, and I_{LO}/I_{2D} is ~0.2, which shows the presence of good quality graphene with excellent surface coverage and low sheet resistance, as we have recently reported [40]. The Raman spectra of the EG surface after MoS_2 synthesis show the appearance of E_{2g} and A_{1g} peaks while the graphene peaks are visible, demonstrating the presence of graphene under the MoS_2 layer (**Figure 2d**). I_D/I_G has appeared unchanged after MoS_2 growth, indicating that no significant new defects are formed during this process. However, I_{LO}/I_{2D} has increased slightly to ~0.26, indicating some loss of graphene (**Figure S5a**). The Raman wavenumber difference between E_{2g} and A_{1g} peaks can be used as an indicator for assessing the number of MoS_2 layers [51, 55]. Here on both surfaces, the E_{2g} and A_{1g} peak distance is ~25 cm^{-1}, corresponding to multi layers (**Figure S5b**) [51, 55]. The alignment of the MoS_2 crystals affects the intensity ratio of E_{2g}/A_{1g} peaks; the out-of-plane mode (A_{1g}) is pronounced when the MoS_2 crystals are vertical due to higher exposure of the edges [56-58]. Here, the E_{2g}/A_{1g} ratio is higher for the MoS_2/SiC electrodes (0.45) compared to the MoS_2/EG (0.37), indicating that MoS_2 crystals are more vertically aligned on the EG surface, which is in agreement with the SEM images. This fact, along with some etching of graphene occurring during the MoS_2 growth, explains also the higher intensity of the Si and SiC peaks.

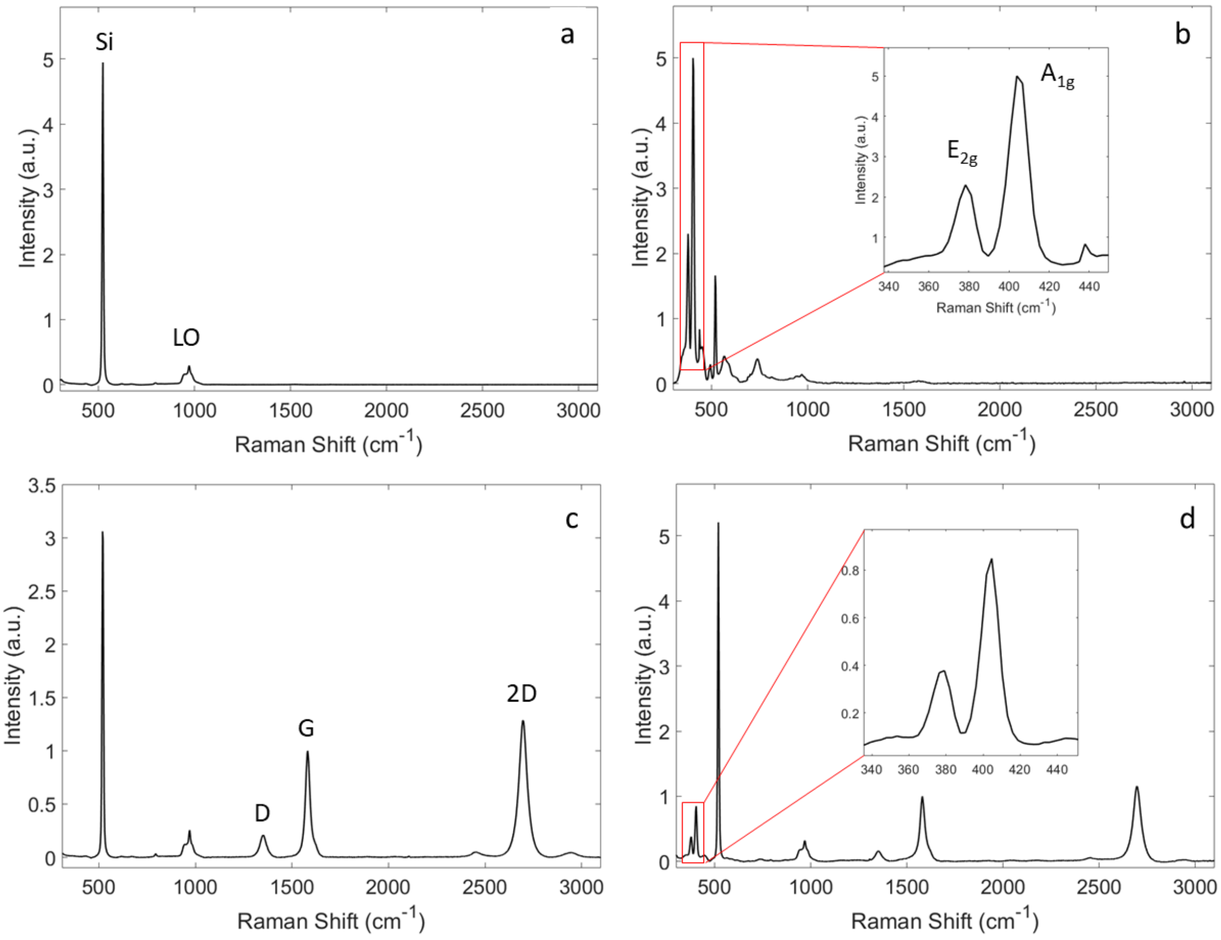

Figure 2. Raman spectra of (a) pristine 3C-SiC/Si substrate, (b) MoS_2 synthesized on the 3C-SiC/Si, (c) EG grown on 3C-SiC/Si substrate, (d) MoS_2 synthesized on the EG electrodes.

High-resolution XPS C 1s spectra of the EG sample show a C-C peak (attributed to graphene) at ~284.7 eV, SiC at ~283 eV, and C-O at ~286 eV (**Figure 3a**). XPS C 1s spectra of the epitaxial graphene sample after the MoS_2 synthesis show the presence of the C-C and Si-C peaks, but the C-O peak has been removed during the MoS_2 growth (**Figure 3b**). We also observe that the intensity of the C-C peak decreases after the MoS_2 growth. Specifically, the ratio of the intensities of the C-C and Si-C peaks decreases by a factor of ~ 6, which indicates that some graphene has been etched away during the growth process. This is in agreement with the I_{LO}/I_{2D} increase observed in the Raman measurements. Mo XPS 3d spectra show two intense peaks of Mo $3d_{5/2}$

(~228 eV) and Mo $3d_{3/2}$ (~231.2 eV), which relate to the Mo (IV) oxydation state of MoS_2, while the less intense peak at ~225.2 eV corresponds to S 2s of MoS_2 (**Figure 3c**) [59]. A less intense doublet at ~231.2/233.8 eV corresponds to the Mo (VI) oxidation state in MoO_3, attributed to some residual oxide present on the surface after MoS_2 growth. The S 2p region indicates the presence of two peaks, S $2p_{3/2}$ (~160.6 eV) and S $2p_{1/2}$ (~162.1 eV), which are characteristic of the Mo-S bonding (**Figure 3d**) [59].

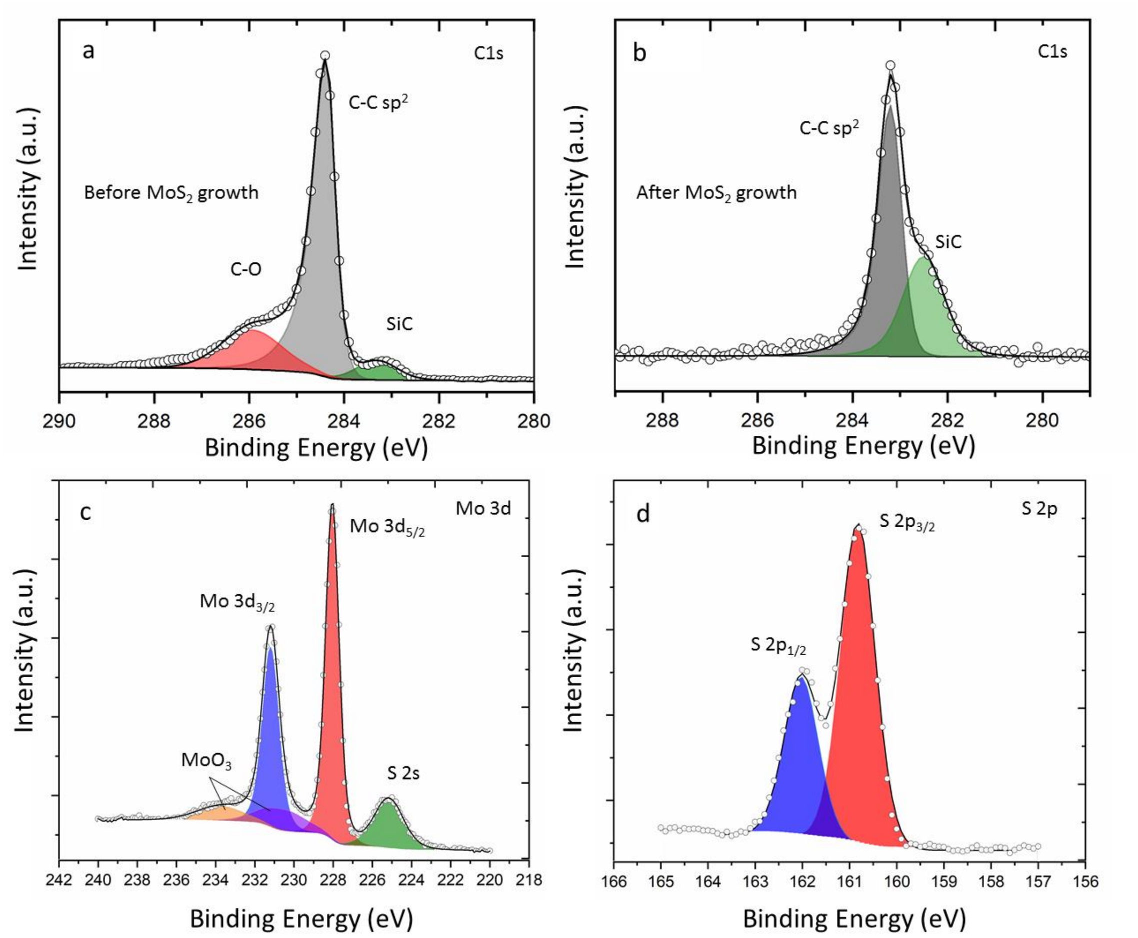

Figure 3. XPS C 1s spectra of (a) EG/3C-SiC/Si, (b) after MoS_2 synthesis. (c) Mo 3d spectra of the electrode after MoS_2 synthesis, (d) S 2p spectra of the same sample.

The CV curve of the cells fabricated with the bare 3C-SiC/Si electrodes shows a quasi-rectangular shape, which is characteristic of double-layer charge storage (**Figure 4a**). The CV tests of the cell with MoS_2/3C-SiC electrodes show a minor improvement in capacitance (**Figure 4b**) compared to the 3C-SiC/Si cell as the area enclosed by the curve is indicative of the charge storage capacity. The CV curves of the cell fabricated using MoS_2/EG hybrid electrodes demonstrate a significant improvement in charge storage, with a more than six-fold increase in the area (**Figure d**). Particularly, the importance of graphene for harnessing the MoS_2 energy storage capabilities becomes evident when comparing the CV test results of the cell fabricated with MoS_2/3C-SiC electrodes with the MoS_2/EG ones (**Figure 4b & d**).

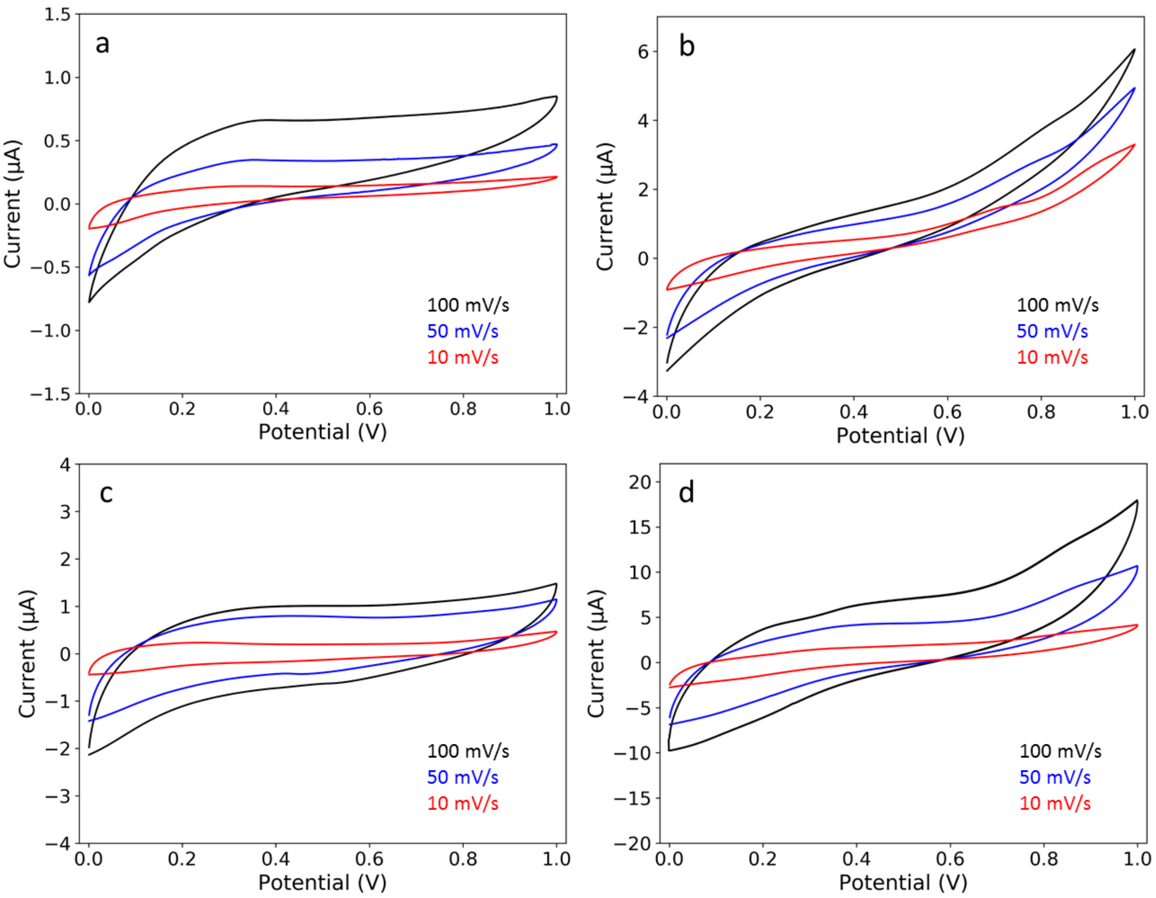

Figure 4. CV curves of the cells fabricated with (a) pristine 3C-SiC/Si, (b) MoS_2 synthesized on the 3C-SiC/Si, (c) EG grown on 3C-SiC/Si, (d) MoS_2 synthesized on the EG. All the CV curves are presented on the same scale to help the comparison. The vertical range in panel d is 5 times that of panel b and c, and 12 times that of panel a, demonstrating the large increase in efficiency.

Figure 5 shows the galvanostatic charge/discharge test results of the cells, and table 1 presents the electrodes' areal specific capacitance calculated based on the charge/discharge test results. The bare 3C-SiC electrodes yield the smallest capacitance. The capacitance of the electrodes made of MoS_2 alone on 3C-SiC (no EG) does not show substantial improvement. However, the cell with electrodes of MoS_2 coupled with EG on 3C-SiC yields a remarkable increase in areal capacitance, from 24 $\mu F/cm^2$ to 554 $\mu F/cm^2$ at 1 μA (**Table 1**). The energy densities (E) are estimated using the relationship $E = \frac{1}{2}\,C\,(\Delta U)^2$. It is interesting to note that although the MoS_2/3C-SiC electrodes offer a significantly higher surface area compared to the EG only electrodes, they show lower capacitance. This indicates the importance of electrode conductivity in charge storage applications of TMS materials. Electrochemical impedance spectroscopy measurement data also indicates that MoS_2/EG electrodes have lower impedance, as expected, compared to MoS_2/3C-SiC electrodes (**Figure S6**). This improvement of the electrode/electrolyte interface impedance has a beneficial effect on the capacitance performance, as seen from the CV and CD data. Having said that, the vertical alignment of the MoS_2 nanosheets on the EG surface drastically limits the total contact area of each MoS_2 with graphene, slowing down charging and charge collection processes at the interface of the two materials. We expect this factor to be a possible reason for the observed distortion in the charge/discharge curves. This hypothesis is corroborated by the fact that the distortion is very pronounced for the cells containing MoS_2 (**Figure 5b and d**), particularly for the MoS_2 on EG cells (**Figure 5d**), where most of the crystals are indeed vertically aligned.

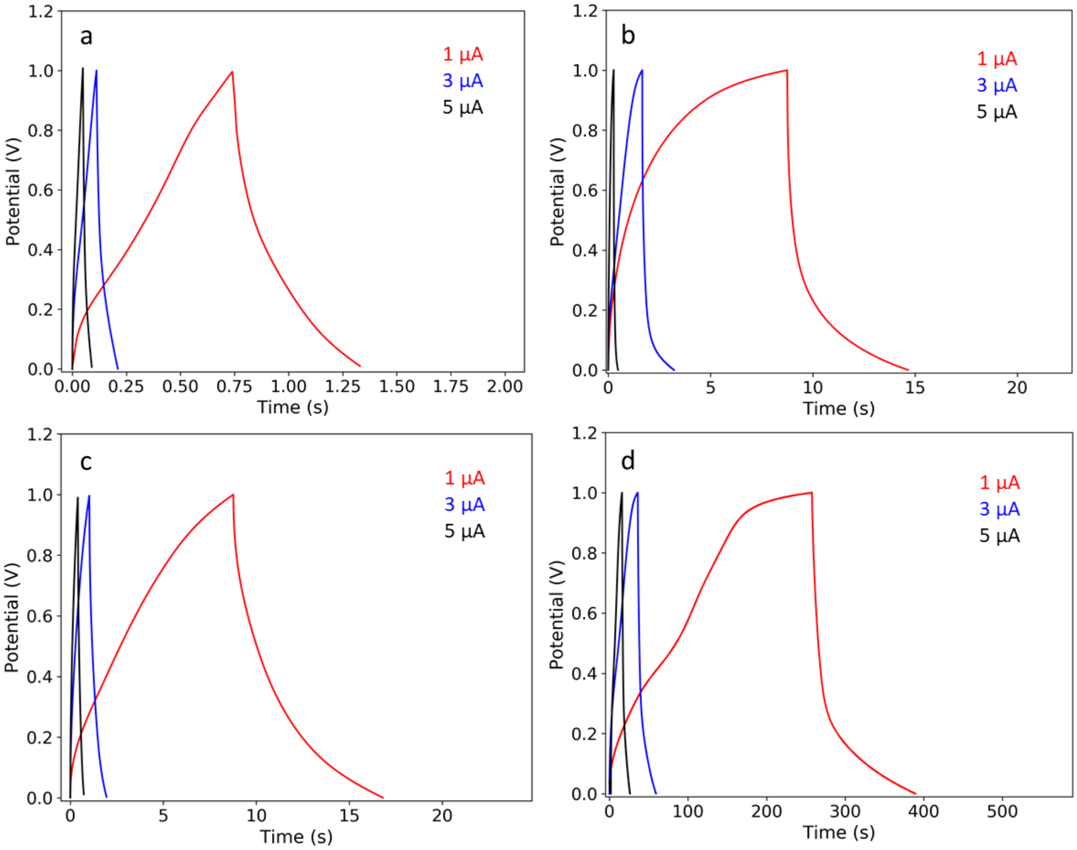

Figure 5. Galvanostatic charge/discharge test result of the cells fabricated with (a) pristine 3C-SiC/Si, (b) MoS_2 synthesized on the 3C-SiC/Si, (c) EG grown on 3C-SiC/Si, (d) MoS_2 synthesized on the EG.

Table 1. The electrodes' specific capacitance calculated from galvanostatic charge/discharge tests and their corresponding energy densities.

Electrode Type	I (μA)	Electrode Type			
		SiC/Si	MoS_2/SiC/Si	Epitaxial Graphene	MoS_2/Epitaxial Graphene
C (μF/cm²)	1	2.5	24	32	554
	3	1.2	18	11	275
	5	1	4	7	190
E(μWh/m²)	1	3.5	33.3	44.4	769.4
	3	1.7	25	15.3	381.9
	5	1.4	5.6	9.7	263.9

The best performing cell, made of MoS_2/EG hybrid electrodes, has been further tested for long cycling charge/discharge. **Figure 6** indicates that the MoS_2/EG electrodes tend to drop about 30% of their performance over 10000 cycles. The capacitance drops by 20% after 2000 cycles, and it only drops further 10% after 8000 cycles (**Figure 6a**). Such retention drop has also been reported for the MoS_2/reduced graphene oxide composite electrodes [11, 20, 60]. However, note that the CV tests of the cell in the initial condition and after 10000 cycles of charge/discharge does not show a significant performance change (**Figure 6b**).

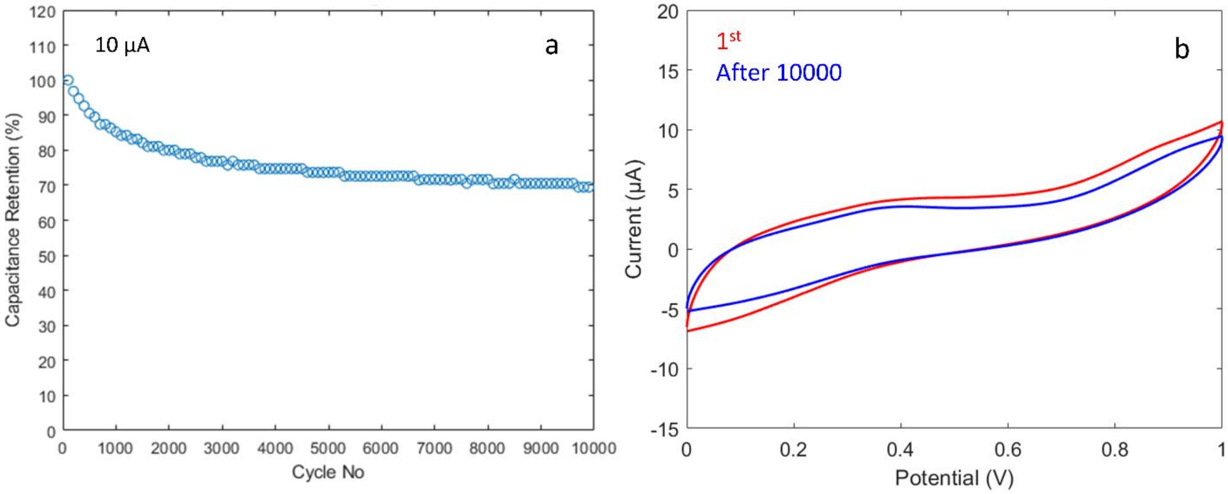

Figure 6. (a) Long cycling galvanostatic charge/discharge test result of the cell fabricated with MoS_2/EG hybrid electrodes, (b) CV curves with 50 mV/s scan rate of the cell at the initial condition and after 10000 charge/discharge tests.

Finally, it should be noted that defective graphenic material is generally superior to low-defect graphene as an electrode for supercapacitors, being more chemically active and providing a higher amount of charge storage sites [8, 41, 44]. However, a highly defective graphenic layer is not efficient in combination with MoS_2 (**Figure S2 and S7**), because of the lack of a highly conductive medium. When used in combination with MoS_2, a highly-conductive and low-defect graphene is necessary to complement the MoS_2 capabilities for energy storage.

4. Conclusions

In summary, we have shown that epitaxial graphene on cubic silicon carbide can complement well the use of transition metal sulfides for miniaturized, on-chip supercapacitors. Epitaxial graphene provides a highly conductive medium for the MoS_2 layer leading to a capacitance improvement of more than 20 times, as compared to electrodes made of MoS_2 alone. A graphene layer with good coverage and low-defect density is key for enabling the charge storage capabilities of the MoS_2 layer. In addition, the epitaxial graphene surface provides a template for prevalently vertical growth of MoS_2 crystals, which also increases the total accessible and active area for energy storage. On the other hand, the vertical alignment of the crystals also limits the contact surface between MoS_2 and graphene, slowing down the charging and charge collection at the interface. We believe that further tuning of the TMS growth temperature could lead to the improvement of the growth orientation achieving a trade-off between an increase in capacitance and responsivity of the system, according to the specific final application.

These insights offer a new path to develop further miniaturized on-chip energy storage systems compatible with silicon electronics based on layered materials, which can support the power demand to operate integrated smart systems.

ACKNOWLEDGMENT

Funding from the Air Force Office for Scientific Research through grant 18IOA052 and from ARC through the Discovery Project DP200102546 is kindly acknowledged. The UTS MAU labs are acknowledged for providing access to the fabrication facilities. This work was also enabled by the Central Analytical Research Facility hosted by the Institute for Future Environments at QUT.

REFERENCES

[1] Z. Niu, L. Zhang, L. Liu, B. Zhu, H. Dong, X. Chen, All‐solid‐state flexible ultrathin micro‐supercapacitors based on graphene, Advanced Materials, 25 (2013) 4035-4042.

[2] C.-H. Chang, B. Hsia, J.P. Alper, S. Wang, L.E. Luna, C. Carraro, S.-Y. Lu, R. Maboudian, High-temperature all solid-state microsupercapacitors based on SiC nanowire electrode and YSZ electrolyte, ACS Applied Materials & Interfaces, 7 (2015) 26658-26665.

[3] J. Li, S. Sollami Delekta, P. Zhang, S. Yang, M.R. Lohe, X. Zhuang, X. Feng, M. Östling, Scalable fabrication and integration of graphene microsupercapacitors through full inkjet printing, ACS Nano, 11 (2017) 8249-8256.

[4] J. Liang, A.K. Mondal, D.-W. Wang, F. Iacopi, Graphene-based planar microsupercapacitors: recent advances and future challenges, Advanced Materials Technologies, 4 (2019) 1800200.

[5] E. Frackowiak, F. Beguin, Carbon materials for the electrochemical storage of energy in capacitors, Carbon, 39 (2001) 937-950.

[6] Y. Zhao, J. Liu, B. Wang, J. Sha, Y. Li, D. Zheng, M. Amjadipour, J. MacLeod, N. Motta, Supercapacitor electrodes with remarkable specific capacitance converted from hybrid graphene Oxide/NaCl/Urea Films, ACS Applied Materials & Interfaces, 9 (2017) 22588-22596.

[7] M. Conte, Supercapacitors technical requirements for new applications, Fuel Cells, 10 (2010) 806-818.

[8] M. Amjadipour, D. Su, F. Iacopi, Graphitic-based solid-state supercapacitors: enabling redox reaction by in situ electrochemical treatment, Batteries & Supercaps, 3 (2020).

[9] J.M. Soon, K.P. Loh, Electrochemical double-layer capacitance of MoS2 nanowall films, Electrochemical and Solid-State Letters, 10 (2007) A250-A254.

[10] L. Cao, S. Yang, W. Gao, Z. Liu, Y. Gong, L. Ma, G. Shi, S. Lei, Y. Zhang, S. Zhang, Direct laser‐patterned micro‐supercapacitors from paintable MoS2 films, Small, 9 (2013) 2905-2910.

[11] T. Wang, S. Chen, H. Pang, H. Xue, Y. Yu, MoS2‐based nanocomposites for electrochemical energy storage, Advanced Science, 4 (2017) 1600289.

[12] P. Sun, R. Wang, Q. Wang, H. Wang, X. Wang, Uniform MoS2 nanolayer with sulfur vacancy on carbon nanotube networks as binder-free electrodes for asymmetrical supercapacitor, Applied Surface Science, 475 (2019) 793-802.

[13] L. Wang, Y. Ma, M. Yang, Y. Qi, Titanium plate supported MoS2 nanosheet arrays for supercapacitor application, Applied Surface Science, 396 (2017) 1466-1471.

[14] H. Sun, H. Liu, Z. Hou, R. Zhou, X. Liu, J.-G. Wang, Edge-terminated MoS2 nanosheets with an expanded interlayer spacing on graphene to boostsupercapacitive performance, Chemical Engineering Journal, 387 (2020) 124204.

[15] Y.-T. Liu, X.-D. Zhu, Z.-Q. Duan, X.-M. Xie, Flexible and robust MoS2–graphene hybrid paper cross-linked by a polymer ligand: a high-performance anode material for thin film lithium-ion batteries, Chemical Communications, 49 (2013) 10305-10307.

[16] H. Wang, H. Feng, J. Li, Graphene and graphene‐like layered transition metal dichalcogenides in energy conversion and storage, Small, 10 (2014) 2165-2181.

[17] D. Sarkar, D. Das, S. Das, A. Kumar, S. Patil, K.K. Nanda, D.D. Sarma, A. Shukla, Expanding Interlayer Spacing in MoS2 for Realizing an Advanced Supercapacitor, ACS Energy Letters, 4 (2019) 1602-1609.

[18] M. Acerce, D. Voiry, M. Chhowalla, Metallic 1T phase MoS2 nanosheets as supercapacitor electrode materials, Nature Nanotechnology, 10 (2015) 313-318.

[19] E.G. da Silveira Firmiano, A.C. Rabelo, C.J. Dalmaschio, A.N. Pinheiro, E.C. Pereira, W.H. Schreiner, E.R. Leite, Supercapacitor electrodes obtained by directly bonding 2D MoS2 on reduced graphene oxide, Advanced Energy Materials, 4 (2014) 1301380.

[20] X. Xie, Z. Ao, D. Su, J. Zhang, G. Wang, MoS2/Graphene composite anodes with enhanced performance for sodium‐ion batteries: the role of the two‐dimensional heterointerface, Advanced Functional Materials, 25 (2015) 1393-1403.

[21] P. Geng, S. Zheng, H. Tang, R. Zhu, L. Zhang, S. Cao, H. Xue, H. Pang, Transition metal sulfides based on graphene for electrochemical energy storage, Advanced Energy Materials, 8 (2018) 1703259.

[22] H.-M. Ji, A.-L. Luan, C.-C. Dai, M. Li, G. Yang, W.-H. Hou, Highly active free-standing and flexible MoS2/rGO sandwich-structured films for supercapacitor applications, Solid State Communications, 297 (2019) 45-49.

[23] H.-U. Kim, M. Kim, Y. Jin, Y. Hyeon, K.S. Kim, B.-S. An, C.-W. Yang, V. Kanade, J.-Y. Moon, G.Y. Yeom, Low-temperature wafer-scale growth of MoS2-graphene heterostructures, Applied Surface Science, 470 (2019) 129-134.

[24] J. Li, K. Liao, X. Wang, P. Shi, J. Fan, Q. Xu, Y. Min, High‐Performance Flexible All‐Solid‐State Supercapacitors Based on Ultralarge Graphene Nanosheets and Solvent‐Exfoliated Tungsten Disulfide Nanoflakes, Advanced Materials Interfaces, 4 (2017) 1700419.

[25] N. Li, T. Lv, Y. Yao, H. Li, K. Liu, T. Chen, Compact graphene/MoS 2 composite films for highly flexible and stretchable all-solid-state supercapacitors, Journal of Materials Chemistry A, 5 (2017) 3267-3273.

[26] M.A. Bissett, I.A. Kinloch, R.A. Dryfe, Characterization of MoS2–graphene composites for high-performance coin cell supercapacitors, ACS Applied Materials & Interfaces, 7 (2015) 17388-17398.

[27] F. Clerici, M. Fontana, S. Bianco, M. Serrapede, F. Perrucci, S. Ferrero, E. Tresso, A. Lamberti, In situ MoS2 decoration of laser-induced graphene as flexible supercapacitor electrodes, ACS Applied Materials & Interfaces, 8 (2016) 10459-10465.

[28] H. Ji, S. Hu, Z. Jiang, S. Shi, W. Hou, G. Yang, Directly scalable preparation of sandwiched MoS2/graphene nanocomposites via ball-milling with excellent electrochemical energy storage performance, Electrochimica Acta, 299 (2019) 143-151.

[29] M. Saraf, K. Natarajan, S.M. Mobin, Emerging Robust Heterostructure of MoS2–rGO for High-Performance Supercapacitors, ACS Applied Materials & Interfaces, 10 (2018) 16588-16595.

[30] M. Amjadipour, A. Tadich, J.J. Boeckl, J. Lipton-Duffin, J. MacLeod, F. Iacopi, N. Motta, Quasi free-standing epitaxial graphene fabrication on 3C–SiC/Si(111), Nanotechnology, 29 (2018) 145601.

[31] N. Mishra, J. Boeckl, N. Motta, F. Iacopi, Graphene growth on silicon carbide: a review, Physica Status Solidi (a), 213 (2016) 2277-2289.

[32] C. Riedl, C. Coletti, U. Starke, Structural and electronic properties of epitaxial graphene on SiC (0 0 0 1): a review of growth, characterization, transfer doping and hydrogen intercalation, Journal of Physics D: Applied Physics, 43 (2010) 374009.

[33] W.A. De Heer, C. Berger, M. Ruan, M. Sprinkle, X. Li, Y. Hu, B. Zhang, J. Hankinson, E. Conrad, Large area and structured epitaxial graphene produced by confinement controlled sublimation of silicon carbide, Proceedings of the National Academy of Sciences, 108 (2011) 16900-16905.

[34] S. Wang, B. Hsia, C. Carraro, R. Maboudian, High-performance all solid-state micro-supercapacitor based on patterned photoresist-derived porous carbon electrodes and an ionogel electrolyte, Journal of Materials Chemistry A, 2 (2014) 7997-8002.

[35] F. Liu, A. Gutes, I. Laboriante, C. Carraro, R. Maboudian, Graphitization of n-type polycrystalline silicon carbide for on-chip supercapacitor application, Applied Physics Letters, 99 (2011) 112104.

[36] B. Hsia, M.S. Kim, M. Vincent, C. Carraro, R. Maboudian, Photoresist-derived porous carbon for on-chip micro-supercapacitors, Carbon, 57 (2013) 395-400.

[37] F. Iacopi, N. Mishra, B.V. Cunning, D. Goding, S. Dimitrijev, R. Brock, R.H. Dauskardt, B. Wood, J. Boeckl, A catalytic alloy approach for graphene on epitaxial SiC on silicon wafers, Journal of Materials Research, 30 (2015) 609-616.

[38] N. Mishra, J.J. Boeckl, A. Tadich, R.T. Jones, P.J. Pigram, M. Edmonds, M.S. Fuhrer, B.M. Nichols, F. Iacopi, Solid source growth of graphene with Ni–Cu catalysts: towards high quality in situ graphene on silicon, Journal of Physics D: Applied Physics, 50 (2017) 095302.

[39] B.V. Cunning, M. Ahmed, N. Mishra, A.R. Kermany, B. Wood, F. Iacopi, Graphitized silicon carbide microbeams: wafer-level, self-aligned graphene on silicon wafers, Nanotechnology, 25 (2014) 325301.

[40] A. Pradeepkumar, M. Amjadipour, N. Mishra, C. Liu, M.S. Fuhrer, A. Bendavid, F. Isa, M. Zielinski, H.I. Sirikumara, T. Jayasekara, D.K. Gaskill, F. Iacopi, p-type epitaxial graphene on cubic silicon carbide on silicon for integrated silicon technologies, ACS Applied Nano Materials, 3 (2019) 830-841.

[41] M. Ahmed, B. Wang, B. Gupta, J.J. Boeckl, N. Motta, F. Iacopi, On-silicon supercapacitors with enhanced storage performance, Journal of The Electrochemical Society, 164 (2017) A638-A644.

[42] M. Portail, M. Zielinski, T. Chassagne, S. Roy, M. Nemoz, Comparative study of the role of the nucleation stage on the final crystalline quality of (111) and (100) silicon carbide films deposited on silicon substrates, Journal of Applied Physics, 105 (2009) 083505.

[43] G. Chichignoud, M. Ucar-Morais, M. Pons, E. Blanquet, Chlorinated silicon carbide CVD revisited for polycrystalline bulk growth, Surface and Coatings Technology, 201 (2007) 8888-8892.

[44] B. Wang, M. Ahmed, B. Wood, F. Iacopi, All-solid-state supercapacitors on silicon using graphene from silicon carbide, Applied Physics Letters, 108 (2016) 183903.

[45] L. Fei, S. Lei, W.-B. Zhang, W. Lu, Z. Lin, C.H. Lam, Y. Chai, Y. Wang, Direct TEM observations of growth mechanisms of two-dimensional MoS2 flakes, Nature Communications, 7 (2016) 1-7.

[46] P. Yang, S. Zhang, S. Pan, B. Tang, Y. Liang, X. Zhao, Z. Zhang, J. Shi, Y. Huan, Y. Shi, Epitaxial growth of centimeter-scale single-crystal MoS2 monolayer on Au (111), ACS Nano, 14 (2020) 5036-5045.

[47] K.V. Bets, N. Gupta, B.I. Yakobson, How the complementarity at vicinal steps enables growth of 2D monocrystals, Nano letters, 19 (2019) 2027-2031.

[48] J. Sitek, J. Plocharski, I. Pasternak, A.P. Gertych, C. McAleese, B.R. Conran, M. Zdrojek, W. Strupinski, Substrate-induced variances in morphological and structural properties of MoS2 grown by chemical vapor deposition on epitaxial graphene and SiO2, ACS Applied Materials & Interfaces, (2020).

[49] F. Iacopi, G. Walker, L. Wang, L. Malesys, S. Ma, B.V. Cunning, A. Iacopi, Orientation-dependent stress relaxation in hetero-epitaxial 3C-SiC films, Applied Physics Letters, 102 (2013) 011908.

[50] B. Gupta, M. Notarianni, N. Mishra, M. Shafiei, F. Iacopi, N. Motta, Evolution of epitaxial graphene layers on 3C SiC/Si (111) as a function of annealing temperature in UHV, Carbon, 68 (2014) 563-572.

[51] C. Lee, H. Yan, L.E. Brus, T.F. Heinz, J. Hone, S. Ryu, Anomalous lattice vibrations of single-and few-layer MoS2, ACS Nano, 4 (2010) 2695-2700.

[52] K. Wang, J. Wang, J. Fan, M. Lotya, A. O'Neill, D. Fox, Y. Feng, X. Zhang, B. Jiang, Q. Zhao, Ultrafast saturable absorption of two-dimensional MoS2 nanosheets, ACS Nano, 7 (2013) 9260-9267.

[53] L. Malard, M. Pimenta, G. Dresselhaus, M. Dresselhaus, Raman spectroscopy in graphene, Physics Reports, 473 (2009) 51-87.

[54] A.C. Ferrari, Raman spectroscopy of graphene and graphite: disorder, electron–phonon coupling, doping and nonadiabatic effects, Solid State Communications, 143 (2007) 47-57.

[55] J. Jeon, S.K. Jang, S.M. Jeon, G. Yoo, Y.H. Jang, J.-H. Park, S. Lee, Layer-controlled CVD growth of large-area two-dimensional MoS 2 films, Nanoscale, 7 (2015) 1688-1695.

[56] Y. Jung, J. Shen, Y. Liu, J.M. Woods, Y. Sun, J.J. Cha, Metal seed layer thickness-induced transition from vertical to horizontal growth of MoS2 and WS2, Nano Letters, 14 (2014) 6842-6849.

[57] D. Kong, H. Wang, J.J. Cha, M. Pasta, K.J. Koski, J. Yao, Y. Cui, Synthesis of MoS2 and MoSe2 films with vertically aligned layers, Nano Letters, 13 (2013) 1341-1347.

[58] F. Lan, Z. Lai, Y. Xu, H. Cheng, Z. Wang, C. Qi, J. Chen, S. Zhang, Synthesis of vertically standing MoS2 triangles on SiC, Scientific Reports, 6 (2016) 1-5.

[59] N. Turner, A. Single, Determination of peak positions and areas from wide - scan XPS spectra, Surface and Interface Analysis, 15 (1990) 215-222.

[60] K. Chang, W. Chen, L-cysteine-assisted synthesis of layered MoS2/graphene composites with excellent electrochemical performances for lithium ion batteries, ACS Nano, 5 (2011) 4720-4728.